IEEE Photonics Journal
An IEEE Photonics Society Publication

Thermal, Modal, and Polarization Features of Double Photonic Crystal Vertical-Cavity Surface-Emitting Lasers

Volume 4, Number 2, April 2012

C. Sciancalepore
B. Ben Bakir
C. Seassal
X. Letartre
J. Harduin
N. Olivier
J.-M. Fedeli
P. Viktorovitch

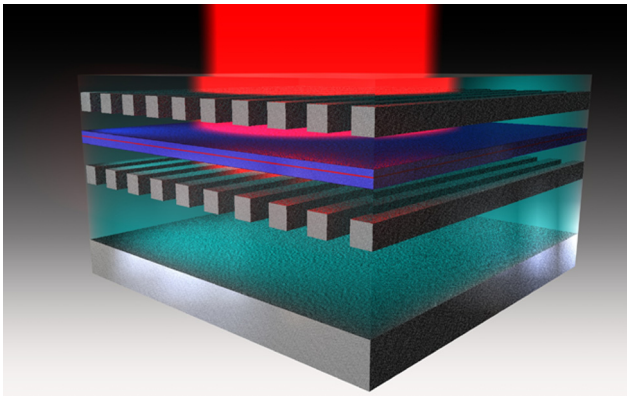

DOI: 10.1109/JPHOT.2012.2189378
1943-0655/$31.00 ©2012 IEEE

Thermal, Modal, and Polarization Features of Double Photonic Crystal Vertical-Cavity Surface-Emitting Lasers

C. Sciancalepore,[1,2] B. Ben Bakir,[2] C. Seassal,[1] X. Letartre,[1] J. Harduin,[2] N. Olivier,[2] J.-M. Fedeli,[2] and P. Viktorovitch[1]

[1]Institut des Nanotechnologies de Lyon, UMR CNRS 5270 Ecole Centrale de Lyon, Université de Lyon, F-69134 Ecully Cedex, France
[2]CEA-LETI Minatec, F-38054 Grenoble Cedex 9, France

DOI: 10.1109/JPHOT.2012.2189378
1943-0655/$31.00 ©2012 IEEE

Manuscript received January 26, 2012; revised February 23, 2012; accepted February 23, 2012. Date of publication February 28, 2012; date of current version March 13, 2012. This work was supported by the European Commission in the framework of the project HELIOS. Corresponding author: C. Sciancalepore (e-mail: corrado.sciancalepore@ec-lyon.fr).

Abstract: Long-wavelength vertical-cavity surface-emitting lasers (VCSELs) for photonics-on-complementary metal–oxide–semiconductor (CMOS) integration based on a double set of Si/SiO_2 photonic crystal mirrors (PCMs) have been recently fabricated. In the present communication, an extensive overview about modal, polarization, and thermal features of optically pumped demonstrators is presented. Capable of operating continuous-wave up to 43 °C at low thresholds, such VCSELs show single-mode polarization-stable operation at 1.55-μm with uncooled output powers in excess of 0.4 mW. This paper aims at singling out notably the device optical features arising from the excellent flexibility of the photonic architecture used. Noticeably, the light molding obtained through the engineering of Si/SiO_2 photonic crystals allows for a tailored modal selection and full polarization control. Furthermore, the high-throughput cost-effective Si-based process technology developed is ideally well-suited for perspective industrial development.

Index Terms: Complementary metal–oxide–semiconductor (CMOS), guided-mode resonance (GMR), photonic crystal (PhC), semiconductor laser, slow Bloch mode (SBM), vertical-cavity surface-emitting laser (VCSEL).

1. Introduction

Long device lifetime, cheap modules and package costs, high-speed modulation capability, and directive radiation pattern allowing easy coupling to single-mode fiber (SMF) through thick multi-mode fiber (MMF) are just some of the key advantageous features characterizing vertical-cavity surface-emitting lasers (VCSELs) [1]. Nowadays, these power-efficient compact semiconductor emitters have already been introduced in a wide-ranging set of developing research fields [2]–[4] and have been steadily present in several mature industrial applications.

Concerning more specifically telecommunication-oriented purposes, VCSELs in the long-wavelength emission bands have been so far mainly targeted for optical interconnects [5], metro-range links [6], coarse wavelength division multiplexing (CWDM) [7], and dense WDM passive optical networking (PON) architectures [8].

Beyond the relevant interest for aforementioned applications, the inherent limit of microelectronics circuits and systems to offer wider modulation bandwidth combined with acceptable power dissipation is going to be attained in the near future, owing to the relentlessly growing demand for

high-speed data transmission and processing. The on-chip back-end integration of photonics functionalities on complementary metal–oxide–semiconductor (CMOS) increasingly appears to be a dynamic research field in the wider silicon photonics [9] proposed to tackle the challenge under such a scenario. VCSELs as compact semiconductor sources constitute the almost ideal solution to address questions of topical interest such as the miniaturization [10] and the fashioning of modal and polarization emission features [11] of existing active components by maintaining good thermal performances, on-chip- as well as free-space-to-fiber optical routing, and, ultimately, a substantial reduction in power consumption.

Nevertheless, active regions in VCSELs for near-infrared emission are generally realized by lattice-matching III–V epi-layers to InP substrates. Within a fully monolithic approach, this implies the epitaxial growth of several-μm-thick phosphide- or InGaAlAs/InAlAs-based distributed Bragg reflectors (DBRs) in order to obtain sufficiently high reflectivity—typically above 99%—that is necessary to reach lasing operation, owing to the small spatial overlap between electromagnetic field and active material representing a distinctive feature of such optical cavities.

Although the wafer bonding of GaAs-based mirrors [12], as well as dielectric reflectors with an enhanced index-contrast [13], constituted a step forward toward increased vertical device compactness and larger stopbands, issues concerning the polarization of emitted light and photons penetration depth were a matter that was still open to debate. While the use of subwavelength surface gratings (SWGs) on DBRs [14], [15] results in device performances which are too sensitive to fabrication parameters drift and laser operating conditions, the introduction of high-index-contrast gratings or, equivalently, photonic crystals (PhCs) [16], [17] as highly reflective polarization-sensitive mirrors marked a turning point in the history of VCSEL technology. Optically [17] and electrically pumped [18] long-wavelength devices using a single PhC layer as output top mirror have been demonstrated over the past few years. Nevertheless, in this paper, we present recently realized VCSEL structures [19] where both reflectors have been substituted with Si/SiO_2 photonic crystal mirrors (PCMs) characterized by nanometer-scale layer thickness, enhanced lateral compactness, broadband reflectivity, and full control over the cavity modal and polarization features. Moreover, PCM-VCSELs fabrication employed standard CMOS pilot line processing tools and high-yield full-wafer bonding [20] of group III–V alloys on silicon, thus combining a flexible device architecture targeting excellent performances with mass-fabrication cost-effective reproducibility.

In this paper, we mainly focused on a thorough assessment of double PCM-VCSELs thermal and optical features. However, the typical use of current apertures and mesa etching in electrically driven emitters introducing additional gain- and index-guiding effects would prevent an exclusive attribution of modal features to the PhC architecture employed. For this reason, optically pumped demonstrators have been fabricated and tested.

This paper is organized as follows. The next section outlines the theoretical pillars for the lightwave manipulation obtained in PCMs, while Section 3 describes the CMOS-compatible technological processing of III–V epitaxial layers on 200-mm silicon-on-insulator (SOI) wafers. Section 4 is devoted to illustrating and discussing devices optical and thermal features. Finally, the last section is dedicated to summarizing the paper's key topics, drawing main conclusions.

2. PCM-VCSELs

The slow-down of the incident lightwave occurring in PhC membranes when exciting surface-addressable slow Bloch modes (SBMs) at flat edges of the folded band structures has already been exploited for the realization of efficient reflectors in optical filters and microlasers [21]–[24]. The control over the polarization of reflected optical waves in 1-D PCMs, as well as the possibility to fully fashion their spectral response [25], [26], make these photonic architectures a versatile building block that can be adopted for a new generation of compact VCSELs displaying full modal and polarization control.

However, the comparative disadvantage of higher thresholds with respect to classic DBR-VCSELs— as correctly pointed out in previous works [17], [18]—poses a serious challenge for the prospects of PCM-based VCSELs, as deviations from design caused by manufacturing imperfections can only partly be blamed.

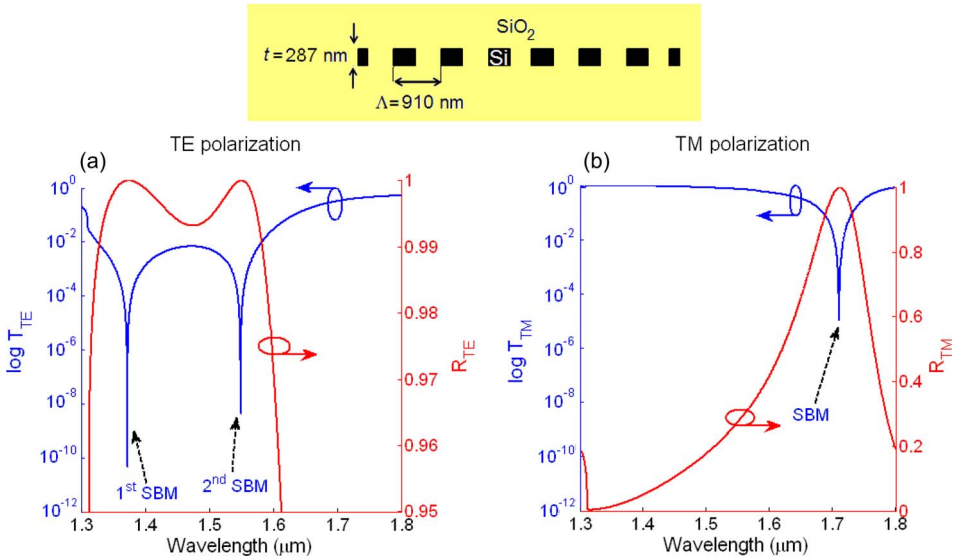

Fig. 1. Si/SiO_2 PCM is 287 nm thick and shows a period of 910 nm and a silicon filling factor of 50%. (a) RCWA-computed reflectivity and transmission spectra of the PCM show two guided-mode resonances supporting a high-reflection band of 247 nm ($R_{TE} > 0.993$) for TE-polarized waves, while a rather weak TM-polarized GMR (b) appears far from the 1.55-μm wavelength region.

As a matter of fact, recent theoretical studies [27]–[30] have provided a deeper insight into the light transport kinetics of slow waves in 1-D PCMs stating a more complete formalism governing their coupling with the incoming electromagnetic field. Radiated photons shined on PCMs couple to SBMs through so-called Fano or, equivalently, guided-mode resonances (GMRs). By design, such resonances can be tailored to exhibit very small lifetimes (i.e., a very low Q factor), which allow recoupling of the most of optical power in phase with the incoming modal lightwave, resulting in a very high reflectivity yield suitable for compact mirrors.

By combining two or more of such low-Q GMRs, highly reflecting mirrors with very large spectral bandwidths are possible, also in the order of several hundreds of nanometers, representing a unique unparalleled feature offered by these photonic structures compared with classical DBRs. The incoming light will excite, though unevenly, those SBMs concurring to originate the mirror stopband. Modal and polarization features of the employed wideband Si/SiO_2 PCM computed by rigorous coupled-wave analysis (RCWA) are reported in Fig. 1.

Double PCM-VCSEL cavities are known to support optical hybrid modes, owing to the hybrid coexistence of a cycling radiated component in between the mirrors and slowly wave-guided photons within mirrors [19], [29], [30].

The inherent anisotropy of the optical medium structuring has direct impact on spatial features of excited modes in 1-D PCMs. In fact, these PhC membranes exhibit strongly anisotropic 2-D dispersion surfaces describing Fano resonances in the reciprocal space. Therefore, when considering lightwave lateral propagation it follows that the band-edge curvature varies accordingly to the wave vector direction, causing the group velocity experienced by wave-guided photons in PCMs to change. This implies that, depending on the propagation direction, optical waves in PCMs can either be efficiently slowed down or more rapidly out-coupled outside the limit area where photons can reradiate reflectively, thus deteriorating the PCM modal reflectivity.

Owing to such strong anisotropy in light kinetics transport, PhC heterostructures have been introduced in PCMs by slightly changing the silicon filling factor and oriented perpendicularly to those directions—here mainly across silicon slits—revealing a faster optical lateral escape rate due to the higher average group velocity [30]. Photons are efficiently reflected by lateral barriers and confined within a photonic crystal well (PCW), being thus prevented to be laterally swept out of the PCM and, in the end, recoupled to the radiated component of hybrid modes. An improved optical

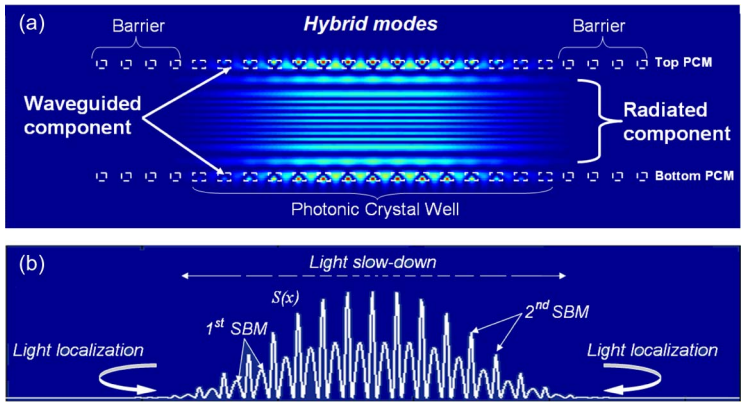

Fig. 2. Three-dimensional finite-difference time-domain (3-D-FDTD) computation of the electromagnetic field intensity in double PCM-VCSELs cavities. (a) Hybrid optical modes sustained by PCM-VCSEL cavities are partly radiated in between the mirrors, as well as wave-guided within photonic crystals. Barriers localize the wave-guided optical field in the PCW, thus increasing the optical energy reemitted in phase with the radiated modal lightwave. (b) Joint action of light localization and slow-down achieved in heterostructure-confined photonic crystal mirrors. The transverse field profile $S(x)$ in the mirror shows that both slow Bloch modes [see Fig. 1(a)] are excited.

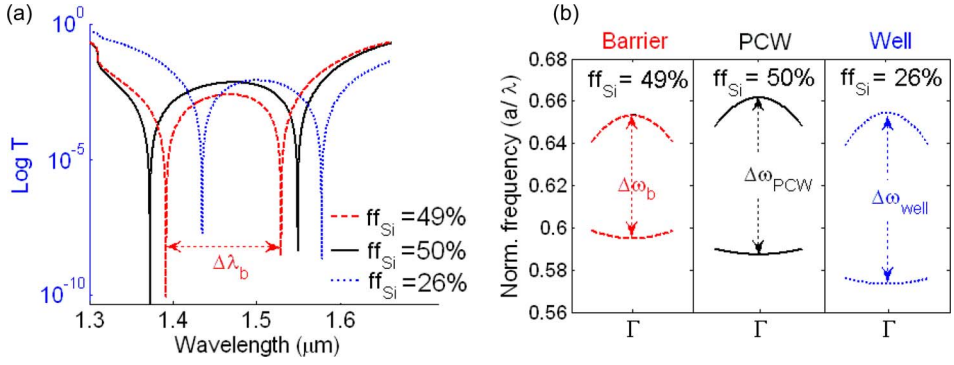

Fig. 3. PCM modal characteristics as function of Si fill-factor. (a) RCWA-computed guided-mode resonances transmittance dips for varying filling factors and (b) corresponding slow Bloch modes dispersion and band-edge curvature at the Γ-point. It can be noted that a photonic heterostructure works as a barrier (red dashed line) for the modes in the PCW (black solid line) only when both modes fall within the PCW band offset $\Delta\omega_{PCW}$. In case one of the two slow Bloch modes drops out of the PCW band offset, the heterostructure behaves as a well (blue dotted line), breaking the mechanism of light localization.

confinement in double PCM-VCSEL cavities is thus achieved through a twofold process of light slow-down and localization in PCMs, providing an inherent reflectivity enhancement of silicon mirrors, as illustrated in Fig. 2.

Notably, it should be here stressed that when adopting photonic heterostructures in PCMs whose stopband arises from two or more mutually interacting GMRs, barriers should be necessarily designed in order to confine all the SBMs excited in the mirror. In order to do so, it proves sufficient to track GMRs wavelengths as a function of the barrier architecture in terms of filling factor and/or period as well as taking clearly into account the band-edge curvature of the corresponding excited SBMs at the Γ-point. With reference to Fig. 3, photonic heterostructures act as barriers on the hybrid mode—therefore enhancing its quality factor—only when the confinement of both SBMs occurs. On the contrary, if by varying the barrier architecture any of these excited modes red- or blue-shifts out of the PCW band offset $(\Delta\omega_{PCW})$, the former behaves as a well, antiguiding the hybrid mode and causing a consistent fall in the resonator quality factor, as reported in [30].

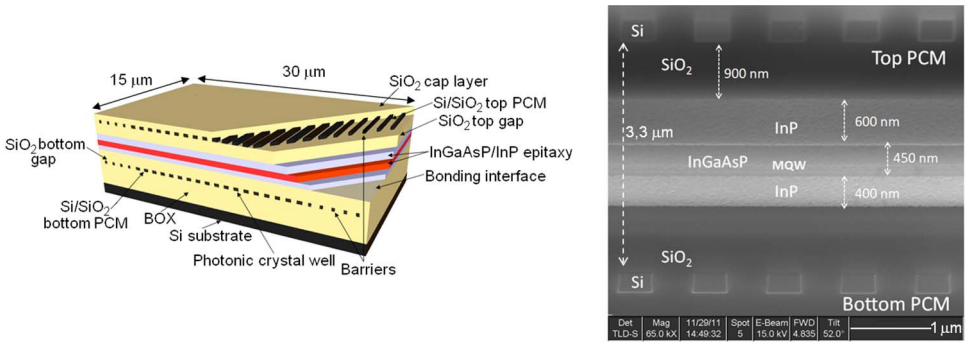

Fig. 4. (Left) Cross-sectional sketch of long-wavelength double PCM-VCSELs for optical pumping along with (right) SEM images. The structure cross section was etched down to the silicon substrate by using focused ion beam (FIB) milling, while a HF-based wet chemical etching was employed in order to reveal silicon bars. The active region consists in three InGaAsP quantum wells tailored for the emission at 1.55 μm.

The structure of Si/SiO_2 optically pumped double PhC VCSELs for long-wavelength emission along with the cross-sectional scanning electron microscope (SEM) view of the device is reported in Fig. 4.

Basically, a 1.4-μm-thick InGaAsP/InP heterostructure is embedded between two silica gaps measuring 900 nm in thickness each, while the structure is vertically terminated by two Si/SiO_2 PCMs and covered by a 500-nm-thick SiO_2 cap layer. Embodying a PhC heterostructure, both reflectors measure almost 290 nm in thickness, showing a periodicity of 910 nm and a silicon filling factor of 50% for the PCW. The reason for silica spacers is ascribable to the necessity to avoid direct evanescent coupling from PCM leaky modes to the laterally wave-guided modes into III–V layers of the laser, which would destroy mirrors reflectivity.

Concerning modal features, the major spatial overlap of higher-order modes with the effective index perturbation step introduced by the PhC barriers results in growing diffraction losses. This can be exploited to perform a selective diffractive confinement of optical modes tailored for single-mode low-threshold lasing operation, without the need to employ any lateral patterning of the III–V active material or invasive post-processing of the PhC membrane. Heterostructure-confined PCMs thus aim at enhancing the optical confinement dramatically, addressing the needs for reduced pumping thresholds, a more comfortable thermal budget, as well as targeting a better control over the VCSEL emission features. Relevant experimental results are presented and discussed in Section 4.

3. CMOS-Compatible 200-mm SOI Fabrication Technology

Affording excellent device performances by employing cost-effective technology for mass-fabrication reproducibility is a key-element for providing authentic industrial potential. Although e-beam efficiency-limited prototyping is commonly used for high-contrast grating definition, we employed exclusively processing tools of a standard CMOS pilot line performing the whole fabrication on 200-mm SOI wafers.

The process can be briefly summarized as follows. 200-mm SOI wafers with a 2-μm-thick buried oxide (BOX) are thermally oxidized down to 290 nm, obtaining the adequate crystalline silicon layer thickness. 248-nm deep ultraviolet (DUV) lithography and HBr-based reactive ion etching (HBr-RIE) are employed for PCMs silicon patterning, while high-density plasma deposition (HDP) is used for both silica spacers, the amorphous silicon top PCM, and the 500-nm cap layer terminating the fabrication process.

Constituting the technological core, the full-wafer molecular bonding of III–V 2-in epitaxial layers to SOI processed wafers has been optimized to the state-of-the-art, obtaining bonding yields well above 90% [20]. An accurate surface treatment through the chemical-mechanical polishing (CMP) of SOI wafers prior to the bonding step, an improved control over the bonding surface contamination

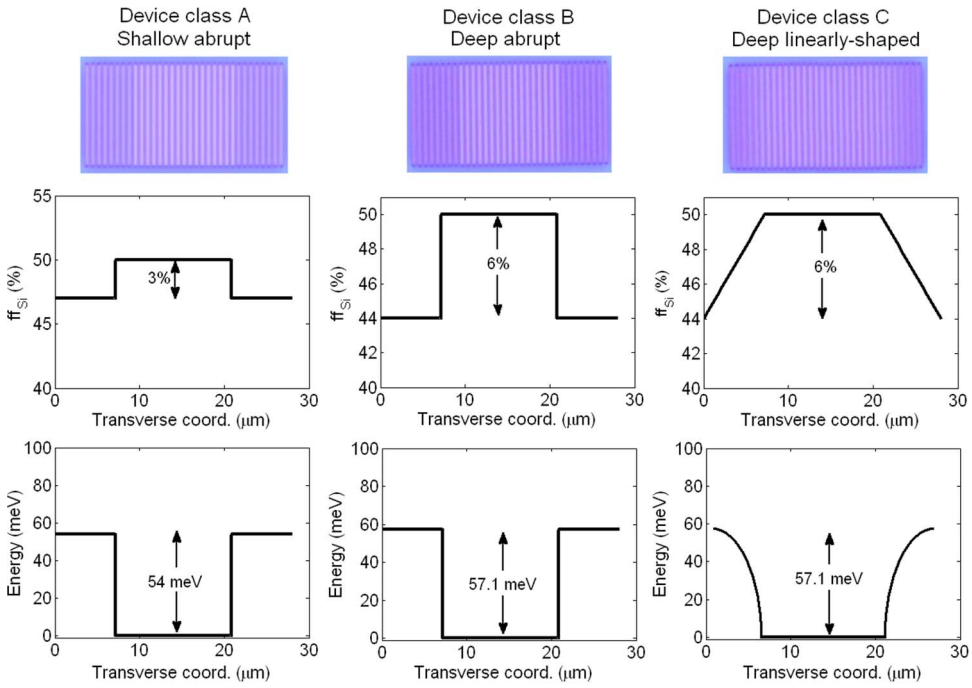

Fig. 5. Optical microscope image of Si/SiO_2 PCMs including different designs of photonic crystal heterostructures. The corresponding variation of the silicon fill-factor and heterostructure band offset along the device transverse section are shown in the series of bottom graphs. A different device class for each barrier design is defined and labeled as A, B, or C.

and roughness, as well as a reduction in both the epitaxial bow and defect density achieved by metalorganic chemical vapor deposition (MOCVD) of group III–V alloys constitute the main reasons behind the achievement. Additional details concerning fabrication and bonding can be found in [19], [30], and references therein.

In order to state a complete description of the effect brought in by photonic heterostructures on the device's optical features, three different PhC barriers design variants—shallow abrupt (device class A), deep abrupt (device class B), and deep linearly shaped (device class C)—have been realized alongside two different dimensions for the squared PCW of 15 μm and 30 μm, respectively. Heterostructures band offsets between PCW and barriers—estimated at the Γ-point—have been calculated by RCWA to be 54 meV and 57.1 meV, respectively, for the shallow and deep heterostructure. Fig. 5 reports the three specific designs of fabricated PCMs.

Heterostructure-confined PhCs are defined at the scale of the 200-mm SOI wafer by a single DUV lithography and RIE step. As mentioned before, it is worth pointing out that no further processing is needed to confer devices with enhanced optical confinement and modal selection, ending up with high-quality performances obtained within the paradigm of a low-cost large-scale fabrication.

4. Double PCM-VCSELs Optical and Thermal Performances

Device testing was performed with a temperature-controlled free-space photoluminescence measurement setup for optical pumping especially conceived for 1.55-μm emitting microlasers.

Owing to the device active region employing InGaAsP 10-nm-thick barriers exhibiting a band offset of 1.17 μm, the lasing wavelength of the pumping diode was set at 1064 nm in order to reduce unnecessary carriers thermalization within the III–V heterostructure, thus enhancing internal quantum efficiency. A thermally stable dichroic mirror showing full transmission at 1550 nm reflects the pumping beam through an objective with numerical aperture (NA) equal to 0.4, being focused

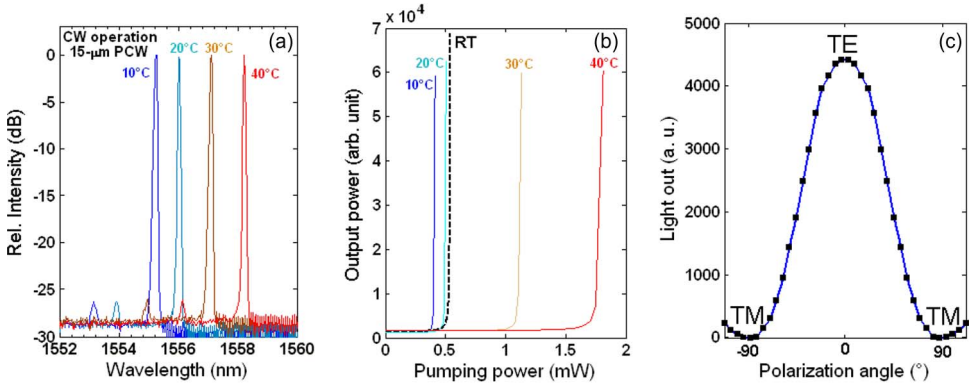

Fig. 6. CW lasing behavior of double PCM-VCSELs at different pumping powers and stage temperatures. (a) Single-mode emission with 26 dB of transverse SMSR is obtained up to a stage temperature of 43 °C. The estimated thermal tuning coefficient is 0.06 nm/K. (b) Light-in–light-out curves corresponding to different stage temperatures. (c) Polarization-resolved spectrum denotes a complete control over polarization emission features.

down to the active region section across the top PCM. Devices have been mounted on a temperature-controlled stage for thermal characterization. The VCSEL lasing signal is then collected back through the same objective lens and collimated into a MMF connected to a spectrometer cooled down to liquid nitrogen temperature for devices optical features acquisition. The pumping beam size has been chosen to fit within the different PCW dimensions and, therefore, focused down to 15- and 30-μm, respectively.

An essential element to be taken into account when evaluating double PCM-VCSEL thresholds and modal selectivity lies in the inefficient pumping of cavity modes. This is caused by the top PCM behaving as an absorbing (estimated amorphous silicon absorption coefficient at 1064 nm $\alpha_{a-Si} = 10\ cm^{-1}$) diffraction grating for the incoming optical waves, introducing undesired distortion in the pumping profile as well as showing considerable power reflectivity at the pumping wavelength. Reported pump powers consider only the power transmitted through the PCM, which we estimate by RCWA and FDTD calculations below 40%–50% of the incident light when the absorption in the PCM is included.

Devices with a 15-μm-wide PCW and deep abrupt barriers (device class B) were firstly tested under continuous-wave excitation at mounting stage temperatures showing room-temperature sub-mW thresholds, a transverse SMSR of 26 dB, a full polarization-controlled emission and lasing up to a stage temperature of 43.6 °C, as reported in Fig. 6. The choice of InGaAsP as active region alloys, notably known for the strong electron leakage occurring at increasing temperature arising from a rather small QW-barrier conduction band offset, actually limits the maximum operation temperature. Furthermore, a laser characteristic temperature T_0 of 40 K has been estimated in our measurements. Pulsed light-in-light–out (LL) curves plotted in Fig. 7 for 500-ns pumping pulses indicate instead the device limit temperature growing to 64 °C at lower thresholds with respect to CW-operation, this being mainly ascribable to the active region heating significantly less when operating in quasi-CW regime.

As shown in Fig. 7(c), the pumping pulses duration clearly affects the transverse SMSR in CW-regime, owing to a thermal lensing effect, which takes place in the device increasingly guiding higher order modes at growing pumping powers per unit time. On the other hand, the laser thermal tuning coefficient $(\partial\lambda/\partial T)$ of 0.06 nm/K extrapolated from the cavity CW-emission at different stage temperatures and constant pumping power denotes a common thermal behavior of the structure, as compared with previous results [18]. It is worth noting that although devices lack monolithic DBRs as well as a metallic heat-sink ensuring thermal dissipation and the III–V part of the VCSEL is surrounded by poorly conductive silica, nevertheless, CW-operation can also be reached under thermal stress at relatively low thresholds. These features confirm the efficient heat sinking around the laser active region, thanks to the unpatterned III–V layers acting as a relief valve for the heat

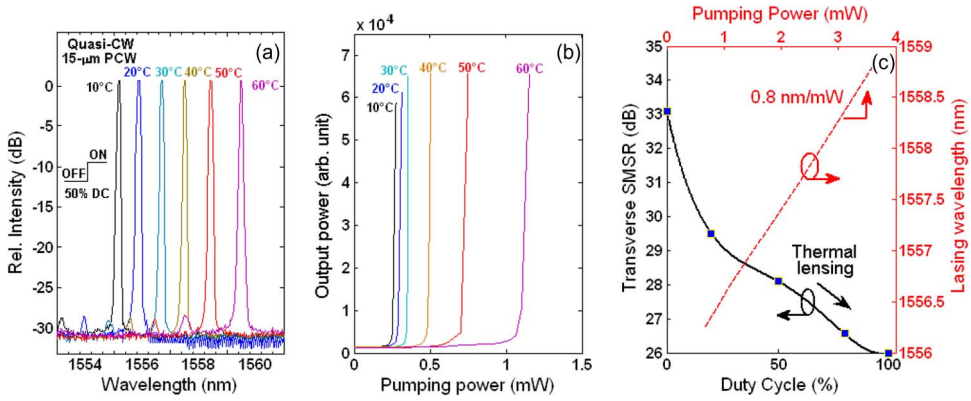

Fig. 7. (a) Quasi-CW lasing behavior of double PCM-VCSELs at different pumping powers (500-ns pumping pulse width, 1-μs pulse period) and stage temperatures. Single-mode emission with 28 dB of transverse SMSR is obtained up to a stage temperature of 64 °C. (b) Corresponding LL curves. (c) Transverse SMSR (solid fitted curve) and CW-lasing wavelength redshift (dashed line) as a function of duty cycle and pumping power, respectively.

propagating laterally along the InP/InGaAsP layers and finally dissipating on a large surface toward the silicon substrate. Moreover, the sub-mW pumping thresholds achieved with the introduction of PhC heterostructures leading to high-Q hybrid modes concur in ameliorating devices thermal budget.

Additionally, the observed emission wavelength redshift as a function of the pumping CW-power of 0.8 nm/mW results in a rather high thermal resistance $R_{\text{th}} = (\partial\lambda/\partial P/\partial\lambda/\partial T) = 13300$ K/W [31], which can be attributed to top PCM severely heating up as a consequence of the pumping scheme used. In fact, as the silicon top PCM absorbs the normal incident radiation, the generated heat cannot find easily its way out of the mirror due to the surrounding silica. The amorphous silicon refractive index changes, inducing a consequent varying phase shift at the reflection and causing the modal emission wavelength to redshift.

In order to understand the effect of barriers architecture and PCW dimensions on both the optical confinement and the transverse SMSR, all design variants (15-μm and 30-μm-wide device class A, B, and C) were compared under CW-pumping at room temperature.

Emission modal features, lasing thresholds and the evolution of the transverse SMSR exhibit deep interweaving with the peculiar perturbation to the PhC effective index introduced by different barrier designs in PCMs. In particular, a stronger variation of the silicon bars width causes an enhanced suppression of higher order modes, thus providing a higher SMSR. This is primarily due to the major spatial overlap of the first- and second-order transverse modes respect to the fundamental mode with the effective index perturbation, generating modal-dependent diffraction losses, resulting in a tailored finely adjustable modal control, as illustrated in Fig. 8.

On the other hand, the increase in perturbation comes at the expense of a slightly higher pumping threshold for the fundamental mode (TE_{00}) determined by increased mode diffraction at PCW boundaries. Instead, the progressive variation of the silicon bars dimension of abrupt barriers (device C) brings in the twofold drawback of a smaller SMSR due to the weaker diffraction occurring at the PCW boundaries and a higher threshold originating from a wider fundamental modal surface in a slightly larger PCW. Devices class A and B show instead both a better modal selection and low pumping thresholds, although the latter look preferable in terms of SMSR, given that the rise in threshold in device B is almost negligible.

A coarser modal selection can be implemented by simply changing the dimension of the PCW. The distance in between the barriers can be used as a control parameter for increasing or decreasing the diffraction suffered by transverse modes, determining single- or multimode operation. As well as that, modes with wider radiation pattern—characterized by a growing transverse wave vector component—experience a higher group velocity arising from the band-edge curvature off the Γ-point, leaking progressively faster out of PCMs. Wider mirrors dimensions and sufficient barriers

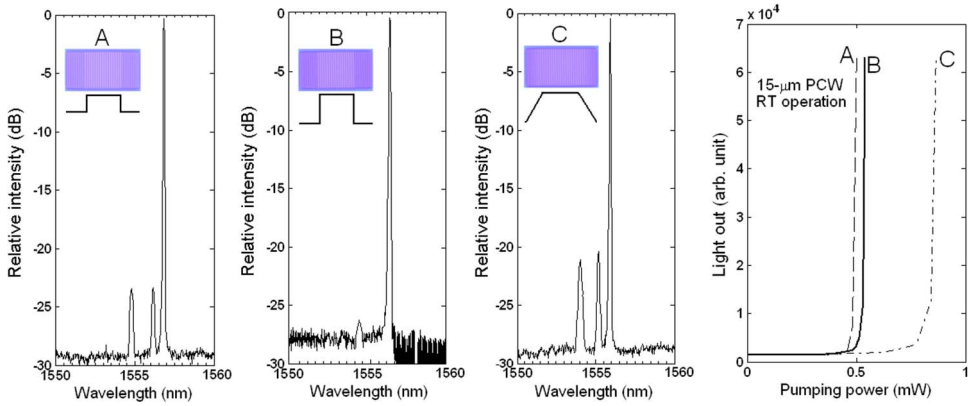

Fig. 8. CW modal behavior of double PCM-VCSELs using different photonic heterostructure design variants. Room-temperature modal features ("A", "B", and "C" insets to the left) and fundamental mode pumping thresholds (rightmost inset) of devices with a shallow abrupt (A), deep abrupt (B), and linearly shaped barriers (C) are shown. Devices with a deep abrupt variation (device class B) of the silicon bars fill-factor provide the better compromise between modal selection (26 dB) and low-threshold operation (0.5 mW).

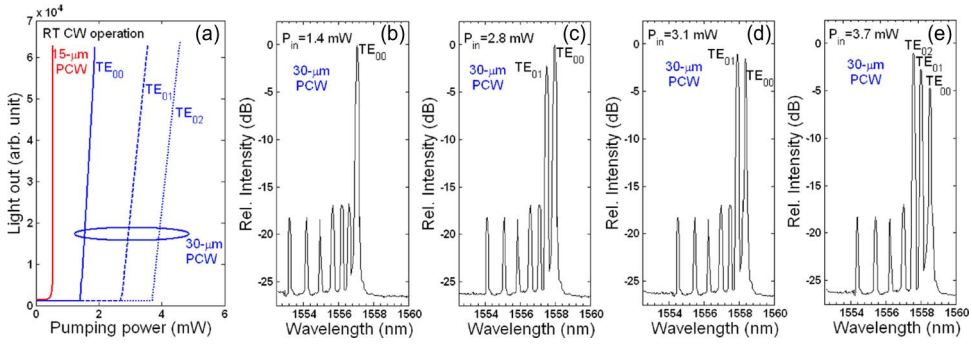

Fig. 9. (a) Room-temperature CW modal behavior of double PCM-VCSELs (device class B) using different PCW dimensions. Fundamental, first- and second-order mode pumping thresholds of class B devices using 15-μm- and 30-μm-wide PCWs are reported. (b)–(e) Room-temperature modal features at different pumping powers of 30-μm-wide double PCM-VCSELs are shown. The concurring onset of spatial hole burning (SHB) and thermal lensing effects, when operating at higher CW-powers, induces higher order modes to prevail over lowest order lasing modes (d), (e).

reflectivity are thus crucial for these modes to lase at relatively low thresholds. Moreover, when using large PCMs, the enlarged cavity transverse boundaries localize optical modes closer to the Γ-point owing to the smaller transverse wave vector, thus benefiting from a further reduction in group velocity. Therefore, wave-guided components of hybrid modes fully exploit the light slow-down when propagating throughout the wider mirror, while only a reduced number of photons is still reflected or diffracted by lateral barriers. In such a case, very high Q factors are possible also for higher order modes.

Relevant comparative results between different PCW sizes for class B devices are shown in Fig. 9. As expected, a larger PCW extends modal volumes requiring higher pumping thresholds [see Fig. 9(a)], while the increased distance between barriers turns off the diffractive selection of the fundamental mode. Moreover, the smaller detuning between different transverse modes observed in larger PCM-VCSELs is the signature of optical modes operating closer to the Γ-point, enjoying a further enhanced slowdown. Notably, the minimal optical losses provided by wider PCMs cause device multimode lasing [see Fig. 9(b)–(d)], while the combined effect of spatial hole burning (SHB)

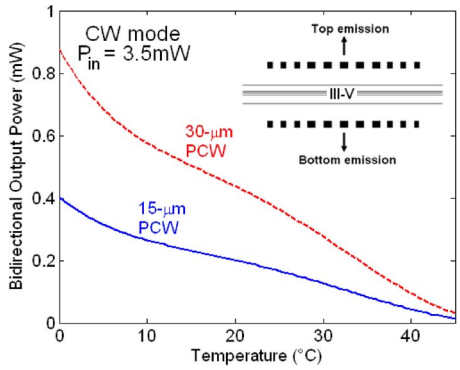

Fig. 10. Double PCM-VCSELs bidirectional global output power (as the sum of both top and bottom emission contributions) fitted curves as a function of stage temperature when operating continuous-mode at a pumping power of 3.5 mW. A room-temperature output power in excess of 0.4 mW is obtained for 30-μm-wide PCW devices.

and thermal lensing occurring at increasing pumping powers determines higher order modes prevailing over the fundamental mode, as reported in Fig. 9(e).

It is now clear that the heterostructure band offset is sufficiently high (above 50 meV) to confine a huge number of transverse modes, while modal selection is introduced by the diffraction experienced by optical modes, owing to the effective index perturbation caused by lateral barriers at the boundaries of the PCW.

Presented results constitute thus a convincing experimental evidence which confirms the flexible role played by photonic heterostructures aimed at a fine manipulation of modal features in double PCM-VCSELs.

Temperature-varying continuous-wave optical output power has been estimated by mounting an infrared power meter along the optical axis of the measurement setup. Considering the symmetry of PCM reflectors and silica gaps, reported measurements consider the global output power as the sum of both top and bottom emission contributions equivalently split into two symmetric beams, as shown in the inset of Fig. 10. Optical losses due to multiple reflections along the optical axis, as well as the output silica/air facet reflectivity, have not been taken into account in the estimates, thus suggesting higher real power levels to be observed in coupled-to-fiber devices endowed with antireflection coatings.

5. Conclusion

Thermal, modal, and polarization features of group III–V VCSELs on silicon employing a double set of PCMs have been presented. Devices operate continuous-wave with submilliwatt thresholds emitting single-mode beams at 1.55-μm with a transverse SMSR of 26 dB, full polarization control, 43 °C maximum operation temperature, and output powers in excess of 0.4 mW for 15-μm-wide PCWs. The architecture of the PhC heterostructure introduced in both PCMs has been exploited to perform a finely adjustable tailoring of the modal selection. The high bonding yields obtained along with the 200-mm CMOS-compatible processing conjugate excellent device performances with cost-effective mass-fabrication standards, indicating strong perspective industrial potential. Higher operation temperatures can be reached by employing AlGaInAs-based alloys lattice-matched to InP for the active region. CMOS-compatible double PCM-VCSELs constitute a robust high-performance building block to be used for the follow-through of silicon photonics, as well as for the technological development of VCSEL photonics.

Acknowledgment

The authors wish to thank M. Garrigues for the valuable contribution concerning the measurement setup and T. Benyattou for the graphic abstract appearing on the cover page.

References

[1] K. Iga, F. Koyama, and S. Kinoshita, "Surface emitting semiconductor laser," *IEEE J. Quantum Electron.*, vol. 24, no. 9, pp. 1845–1855, Sep. 1988.

[2] B. Kögel, H. Halbritter, S. Jatta, M. Maute, G. Böhm, M.-C. Amann, M. Lackener, M. Schwarzott, F. Winter, and P. Meissner, "Simultaneous spectroscopy of NH_3 and CO using a $>$ 50 nm continuously tunable MEMS-VCSEL," *IEEE Sens. J.*, vol. 7, no. 11, pp. 1483–1489, Nov. 2007.

[3] T. Svensson, M. Andersson, L. Rippe, S. Svanberg, S. Andersson-Engels, J. Johansson, and S. Folestad, "VCSEL-based oxygen spectroscopy for structural analysis of pharmaceutical solids," *Appl. Phys. B, Laser Opt.*, vol. 90, no. 2, pp. 345–354, Feb. 2008.

[4] E. Bosman, J. Missinne, B. Van Hoe, G. Van Steenberge, S. Kalathimekkad, J. Van Erps, I. Milenkov, K. Panajatov, T. Van Gijseghem, P. Dubruel, H. Thienpont, and P. Daele, "Ultrathin optoelectronic device packaging in flexible carriers," *IEEE J. Sel. Topics Quantum Electron.*, vol. 17, no. 3, pp. 617–628, May/Jun. 2011.

[5] W. Hofmann, P. Moser, P. Wolf, A. Mutig, M. Kroh, and D. Bimberg, "44 Gb/s VCSEL for optical interconnects," in *Proc. OFC/NFOEC*, Mar. 2011, pp. 1–3.

[6] M.-C. Amann and W. Hoffmann, "InP-based long-wavelength VCSELs and VCSEL arrays," *IEEE J. Sel. Topics Quantum Electron.*, vol. 15, no. 3, pp. 861–868, May/Jun. 2009.

[7] A. Syrbu, A. Mircea, A. Mereuta, A. Caliman, C.-A. Berseth, G. Suruceanu, V. Iakovlev, M. Achtenhagen, A. Rudra, and E. Kapon, "1.5-mW single-mode operation of wafer-fused 1550-nm VCSELs," *IEEE Photon. Technol. Lett.*, vol. 16, no. 5, pp. 1230–1232, May 2004.

[8] W. Hofmann, E. Wong, G. Böhm, M. Ortsiefer, N. H. Zhu, and M.-C. Amann, "1.55-μm VCSEL arrays for high-bandwidth WDM-PONs," *IEEE Photon. Technol. Lett.*, vol. 20, no. 4, pp. 291–293, Feb. 2008.

[9] G. T. Reed, "The optical age of silicon," *Nature*, vol. 427, no. 6975, pp. 595–596, Feb. 2004.

[10] B. Ben Bakir, A. Descos, N. Olivier, D. Bordel, P. Grosse, E. Augendre, L. Fulbert, and J.-M. Fedeli, "Electrically driven hybrid Si/III–V Fabry–Pérot lasers based on adiabatic mode transformers," *Opt. Exp.*, vol. 19, no. 11, pp. 10 317–10 325, May 2011.

[11] F. Mandorlo, P. Rojo-Romeo, X. Letartre, R. Orobtchouk, and P. Viktorovitch, "Compact modulated and tunable microdisk laser using vertical coupling and a feedback loop," *Opt. Exp.*, vol. 18, no. 19, pp. 19 612–19 625, Sep. 2010.

[12] A. Mereuta, G. Suruceanu, A. Caliman, V. Iakovlev, A. Sirbu, and E. Kapon, "10-Gb/s and 10-km error-free transmission up to 100 °C with 1.3-μm wavelength wafer-fused VCSELs," *Opt. Exp.*, vol. 17, no. 15, pp. 12 981–12 986, Jul. 2009.

[13] W. Hofmann, M. Müller, A. Nadtochiy, C. Meltzer, A. Mutig, G. Böhm, J. Rosskopf, D. Bimberg, M.-C. Amann, and C. Chang-Hasnain, "22 Gb/s long wavelength VCSELs," *Opt. Exp.*, vol. 17, no. 20, pp. 17 547–17 554, Sep. 2009.

[14] J. Gustavsson, Å. Haglund, J. Vukušić, J. Bengtsson, P. Jedrasik, and A. Larsson, "Efficient and individually controllable mechanisms for mode and polarization selection in VCSELs, based on a common, localized, sub-wavelength surface grating," *Opt. Exp.*, vol. 13, no. 17, pp. 6626–6634, Aug. 2005.

[15] P. Debernardi, J. M. Ostermann, M. Feneberg, C. Jalics, and R. Michalzik, "Reliable polarization control of VCSELs through monolithically integrated surface gratings: A comparative theoretical and experimental study," *IEEE J. Sel. Topics Quantum Electron.*, vol. 11, no. 1, pp. 107–116, Jan./Feb. 2005.

[16] M. C. Y. Huang, Y. Zhou, and C. J. Chang-Hasnain, "A surface-emitting laser incorporating a high-index-contrast subwavelength grating," *Nat. Photon.*, vol. 1, no. 2, pp. 119–122, Feb. 2007.

[17] S. Boutami, B. Ben Bakir, J.-L. Leclercq, and P. Viktorovitch, "Compact and polarization controlled 1.55-μm vertical-cavity surface-emitting laser using single-layer photonic crystal mirror," *Appl. Phys. Lett.*, vol. 91, no. 7, pp. 071105-1–071105-3, Aug. 2007.

[18] W. Hofmann, C. Chase, M. Muller, Y. Rao, C. Grasse, G. Böhm, M.-C. Amann, and C. Chang-Hasnain, "Long-wavelength high-contrast grating vertical-cavity surface-emitting laser," *IEEE Photon. J.*, vol. 2, no. 3, pp. 415–422, Jun. 2010.

[19] C. Sciancalepore, B. B. Bakir, X. Letartre, J. Harduin, N. Olivier, C. Seassal, J.-M. Fedeli, and P. Viktorovitch, "CMOS-compatible ultra-compact 1.55-μm emitting VCSEL using double photonic crystal mirrors," *IEEE Photon. Technol. Lett.*, vol. 24, no. 6, pp. 455–457, Mar. 2012.

[20] C. Sciancalepore, B. Ben Bakir, X. Letartre, N. Olivier, D. Bordel, C. Seassal, P. Rojo-Romeo, P. Regreny, J.-M. Fedeli, and P. Viktorovitch, "CMOS-compatible integration of III–V VCSELs based on double photonic crystal reflectors," in *Proc. 8th IEEE Int. Conf. GFP*, Sep. 2011, pp. 205–207.

[21] H. Hattori, X. Letartre, C. Seassal, P. Rojo-Romeo, J. Leclercq, and P. Viktorovitch, "Analysis of hybrid photonic crystal vertical cavity surface emitting lasers," *Opt. Exp.*, vol. 11, no. 15, pp. 1799–1808, Jul. 2003.

[22] X. Letartre, J. Mouette, J.-L. Leclerq, P. Rojo-Romeo, C. Seassal, and P. Viktorovitch, "Switching devices with spatial and spectral resolution combining photonic crystal and MOEMS structures," *J. Lightw. Technol.*, vol. 21, no. 7, pp. 1691–1699, Jul. 2003.

[23] S. Boutami, B. B. Bakir, H. Hattori, X. Letartre, J.-L. Leclercq, P. Rojo-Romeo, M. Garrigues, C. Seassal, and P. Viktorovitch, "Broadband and compact 2-D photonic crystal reflectors with controllable polarization dependence," *IEEE Photon. Technol. Lett.*, vol. 18, no. 7, pp. 835–837, Apr. 2006.

[24] S. Boutami, B. Ben Bakir, J.-L. Leclercq, X. Letartre, P. Rojo-Romeo, M. Garrigues, P. Viktorovitch, I. Sagnes, L. Legratiet, and M. Strassner, "Highly selective and compact tunable MOEMS photonic crystal Fabry–Perot filter," *Opt. Exp.*, vol. 14, no. 8, pp. 3129–3137, Apr. 2006.

[25] Y. Ding and R. Magnusson, "Resonant leaky-mode spectral-band engineering and device applications," *Opt. Exp.*, vol. 12, no. 23, pp. 5661–5674, Nov. 2004.

[26] R. Magnusson and M. Shokooh-Saremi, "Physical basis for wideband resonant reflectors," *Opt. Exp.*, vol. 16, no. 5, pp. 3456–3462, Mar. 2008.

[27] P. Viktorovitch, B. Ben Bakir, S. Boutami, J.-L. Leclercq, X. Letartre, P. Rojo-Romeo, C. Seassal, M. Zussy, L. Di Cioccio, and J.-M. Fedeli, "3D harnessing of light with 2.5D photonic crystals," *Laser Photon. Rev.*, vol. 4, no. 3, pp. 401–413, Apr. 2010.
[28] V. Karagodsky, F. G. Sedgwick, and C. J. Chang-Hasnain, "Theoretical analysis of subwavelength high contrast grating reflectors," *Opt. Exp.*, vol. 18, no. 16, pp. 16 973–16 988, Aug. 2010.
[29] S. Boutami, B. Ben Bakir, X. Letartre, J.-L. Leclercq, and P. Viktorovitch, "Photonic crystal slab mirrors for an ultimate vertical and lateral confinement of light in vertical Fabry–Perot cavities," in *Proc. SPIE*, 2008, vol. 6989, p. 69 890V.
[30] C. Sciancalepore, B. Ben Bakir, X. Letartre, J.-M. Fedeli, N. Olivier, D. Bordel, C. Seassal, P. Rojo-Romeo, P. Regreny, and P. Viktorovitch, "Quasi-3D light confinement in double photonic crystal reflectors VCSELs for CMOS-compatible integration," *J. Lightw. Technol.*, vol. 29, no. 13, pp. 2015–2024, Jul. 2011.
[31] A. Bachmann, S. Arafin, and K. Kashani-Shirazi, "Single-mode electrically pumped GaSb-based VCSELs emitting continuous-wave at 2.4 and 2.6 μm," *New J. Phys.*, vol. 11, pp. 125014-1–125014-17, Dec. 2009.